A Visualization Framework for Multi-scale Coherent Structures in Taylor-Couette Turbulence

Duong B. Nguyen, Rodolfo Ostilla Monico, and Guoning Chen

Abstract—Taylor-Couette flow (TCF) is the turbulent fluid motion created between two concentric and independently rotating cylinders. It has been heavily researched in fluid mechanics thanks to the various nonlinear dynamical phenomena that are exhibited in the flow. As many dense coherent structures overlap each other in TCF, it is challenging to isolate and visualize them, especially when the cylinder rotation ratio is changing. Previous approaches rely on 2D cross sections to study TCF due to its simplicity, which cannot of certain attributes and the placement of integral curves/surfaces, usually produce cluttered visualization. To address this challenge and to support domain experts in the analysis of TCF, we developed a visualization framework to separate large-scale structures from the dense, small-scale structures and provide an effective visual representation of these structures. Instead of using a single physical attribute as the standard approach which cannot efficiently separate structures in different scales for TCF, we adapt the feature level-set method to combine multiple attributes and use them as a filter to separate large- and small-scale structures. To visualize these structures, we apply the iso-surface extraction on the kernel density estimate of the distance field generated from the feature level-set. The proposed methods successfully reveal 3D large-scale coherent structures of TCF with different control parameter settings, which are difficult to achieve with the conventional methods.

Index Terms—Flow visualization, Taylor-Couette turbulence, coherent structures



1 Introduction

Taylor-Couette flow (TCF) is the fluid motion between two coaxial, independently rotating cylinders. TCF has become an important model system in fluid dynamics, because it helps to understand the development of hydrodynamic stabilities and pattern formation. Thanks to the simple geometry of the system, fluid mechanics experts can set up a well-controlled experiment to study fundamental nonlinear dynamical phenomena in fluid flows; thus, TCF has become a canonical experiment for the study of shear turbulence. Some practical applications of TCF include solvent extraction in chemical engineering [24] and heat transfer in electric motors [13].

TCF is linearly unstable when angular momentum decreases with radius, and different configurations of inner and outer cylinder rotation lead to diverse dynamics. At low Reynolds numbers, TCF is dominated by a stacking of large-scale structures called Taylor vortices, which arise due to centrifugal instabilities and fill the entire gap between the cylinders. As the Reynolds number increases, and the flow becomes turbulent, structures with increasingly smaller length- and time-scales appear. The large-scale vortices remain, and are relatively stationary in time (e.g., Figure 1(a)). In addition to the theory that large structures depend on the Reynolds numbers, the recent statistic-based method [14] indicates that the turbulent rolls may re-appear with different cylinder rotation ratios R_{Ω} , as also shown in our later results. Nonetheless, the large-scale structures (e.g., Taylor vortices or other coherent structures) modulate the appearance of small-scale structures, and can act as transport barriers; thus, they are particularly interesting to the domain experts. In practice, rather than studying the configurations of the individual vortices (or other small-scale structures) themselves, the spatial distributions of these structures in different scales (especially in large-scale) are of interest in the analysis of TCF.

To identify the different scale structures in TCF, domain experts traditionally rely on the rudimentary visualization techniques (e.g.,

- Duong B. Nguyen is with University of Houston. E-mail: duongnguyenbinh@gmail.com.
- Rodolfo Ostilla Monico is with University of Houston. E-mail: rostilla@central uh edu
- Guoning Chen is with University of Houston. E-mail: chengu@cs.uh.edu.

Manuscript received xx xxx. 201x; accepted xx xxx. 201x. Date of Publication xx xxx. 201x; date of current version xx xxx. 201x. For information on obtaining reprints of this article, please send e-mail to: reprints@ieee.org. Digital Object Identifier: xx.xxxx/TVCG.201x.xxxxxxx

volume rendering, iso-surfacing, and thresholding) based on the physical attributes, such as vorticity or Q-criterion [11]. As illustrated in Figure 2, different parameter settings (here, different threshold values for Q) may lead to structures with significantly different shapes and density, making the identification and tracking of the desired structures difficult. Making this worse is that attributes such as vorticity and Q-criterion in small structures have different value ranges from those in large structures as reported previously [39]. Often, high positive Q-criterion corresponds to vortices with small-scale structures due to its definition, i.e., it is based on vorticity and strain which are inherently local and small-scale quantities, while small Q values may exist both inside and outside the large structures. Furthermore, as shown later (Figure 5), one single attribute with one single threshold value is not sufficient to clearly separate multi-scale coherent structures, especially when the cylinder rotation ratio changes. All these challenges force the fluid mechanic researchers to resort to the visualization of 2D cross section (Figure 1 (a)) through cylinders for TCF analysis, losing important 3D configuration information of the structures. To the best of our knowledge, no existing works provide an effective 3D visualization of TCF that separates the large- and small-scale structures to aid the study of the re-appearance of certain coherent structures (especially, Taylor vortices) in TCF under different rotation ratios.

To address this challenge, we propose a first 3D visualization framework that enables the clear separation of large- and small- scale structures in TCF. To overcome the limitation of the separation of structures in different scales with a single attribute, our framework employs multiple attributes for feature extraction and separation. This is also supported by a recent work on 2D TCF [31] that shows that streamwise velocity aligns reasonably well with the position of the Taylor roll in the flow domain. By extending the feature level-set method [16] to take into account values in a range, we can combine the characteristics of multiple attributes in one analysis to increase the difference between the small- and large- scale structures, making their separation easier and more accurate. To extract a 3D surface representation for the coherent structures, we construct iso-surfaces from the kernel density estimate of the distance field obtained from the feature level-set. Considering the characteristic that TCF with certain rotation ratio may be depicted by its 2D cross sections, referred to as the WS planes formed by the wall-normal and spanwise directions (Figure 1 (a)(c)), we compute the 2D summary configuration of vortices in TCF by projecting the 3D information onto the WS plane. Compared to the visualizations generated with the conventional approaches in both 2D and 3D, our method produces a much cleaner visualization. Our framework is implemented

in CUDA, making it suitable for the efficient analysis of TCF.

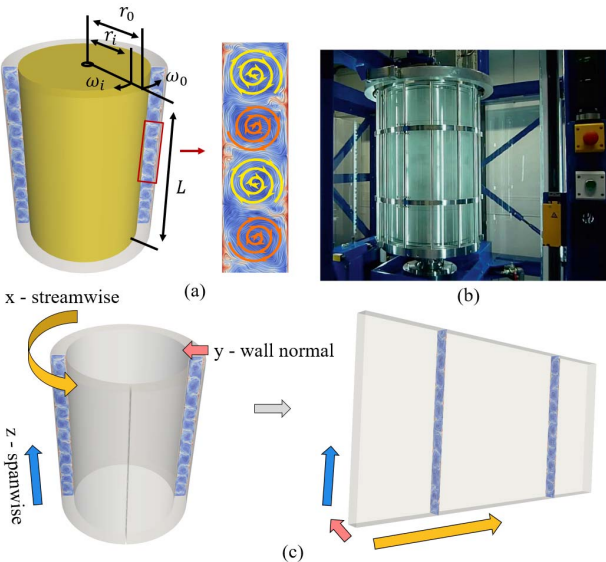


Fig. 1. (a) The Taylor-Couette system consists of two coaxial cylinders, which have an inner cylinder with radius of r_i and an outer cylinder with radius of r_o . Both cylinders are of height L. The inner cylinder rotates with an angular velocity ω_i and the outer cylinder rotates with an angular velocity of ω_o . (b) Twente Turbulent Taylor-Couette (T3C) experimental facility [26]. (c) Domain transformation from the cylindrical to the Cartesian coordinate.

Our framework has been applied to three different TCFs simulated with different control parameters. These three TCFs have different levels of turbulence, making the separation of large-scale structures from the small ones extremely challenging. Our framework successfully reveals the configurations of large-scale coherent structures in all three TCFs. This is the first time the large-scale structures in TCFs are visualized in 3D. From these new visualizations, domain experts not only can see a clear separation of large- and small- scale structures, but they also can see the 3D configuration of large-scale structures in TCFs with low cylinder rotation ratios to better understand the procedure of the formation of Taylor rolls (or Taylor vortices). The efficient computation of our framework will enable the study of the impact of the rotation ratio to the 3D configuration of Taylor rolls in a finer scale and set up the foundation for the study of the time-dependent behavior of TCFs in the future.

2 BACKGROUND

In this section we provide the numerical setup to simulate Taylor-Couette flow (TCF) used in this work and review existing works on vortex detection and visualization frameworks for turbulent flow.

2.1 Numerical Simulation details

In the limit of vanishing curvature, which is more amenable to analysis, Taylor-Couette can be described as the flow between two parallel plates separated by a distance d, which move with equal, but opposite velocities $\pm U/2$. To represent the different rotations of the cylinders, a solid body rotation Ω is added in the spanwise direction. The two non-dimensional parameters that define the flow are the (shear) Reynolds number Re = Ud/v, where v is the kinematic viscosity of the fluid, and the rotation number $R_{\Omega} = 2d\Omega/U$. A schematic of the flow is shown in Figure 3. We fix $Re_s = 10^4$, and vary from $R_{\Omega} = 0$ to $R_{\Omega} = 0.1$, which generate a sufficiently diverse range of length-scales, while also featuring fixed Taylor vortices [31].

To perform the direct numerical simulations, we solve the Navier-Stokes equation using a second-order energy-conserving finite difference code [45]. The two wall-parallel directions are taken as periodic, with periodicity lengths $L_x = 25.12d$ and $L_z = 12.56d$ respectively. This means that the simulation covers a subset of the spatio-temporal domain, $[0,25.12] \times [0,1] \times [0,12.56]$. The resolution of the simulation

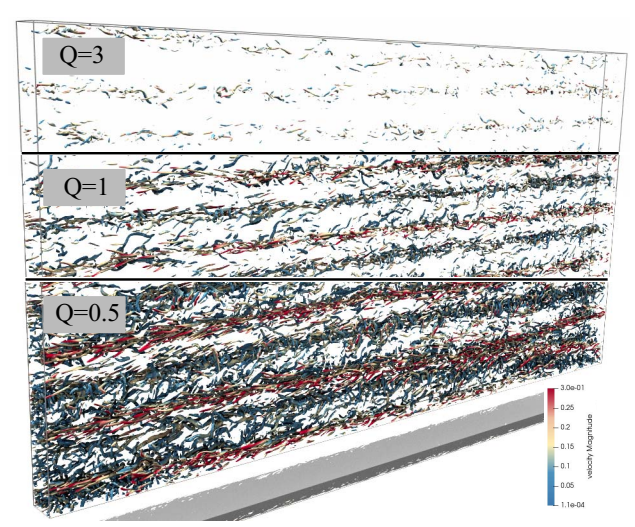


Fig. 2. Traditional issues with Q threshold selection. Domain experts rely on the Q-criterion to extract the vortices and suffer from the issues with the occlusion, because many different scale vortices overlap each others. Note that while visually these dense layouts of vortices form groups that may indicate the formation of Taylor rolls/vortices, they do not align with the location of Taylor vortices as indicated by the velocity field as illustrated in Figure 1 (a).

is $1024 \times 384 \times 1024$ (i.e., the number of grid points in the x,y and z dimension.). The simulation is time-dependent. However, due to the large data size and the complexity of the flow, this work focuses on a single instantaneous snapshot in the statistically stationary regime.

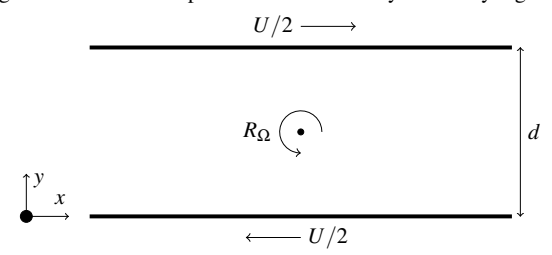


Fig. 3. Schematic of the simulation domain. The third (spanwise) dimension z is omitted for clarity.

2.2 Related Works

There is a large body of literature on the analysis and visualization of flow data [11, 19, 20]. In this section, we focus on the most closely-related works which includes the vortex detection methods and existing visualization frameworks for turbulent flow in general, and for Taylor-Couette flow in particular.

2.2.1 Vortex Detection

Most vortex definitions [11] include two concepts that are still actively researched to this day: (1) vortex coreline – a line or curve that any mass of fluid moving around [21] and (2) an appropriate reference frame so that when instantaneous streamlines mapped onto a plane normal to the vortex core they exhibit a roughly circular or spiral pattern [30]. Based on these two concepts, there are several groups of methods that identify the vortex corelines and vortex regions, respectively.

Region-based methods identify a volume of vortex-like behavior based on some physical attributes, such as pressure [15], vorticity, helicity, Q-criterion, Okubo-Weiss criterion and λ_2 criterion [11]. Most region-based methods require the selection of threshold, which may miss vortices with smaller values. **Line-based methods** focus on the extraction of corelines of vortices. In steady flow, corelines can be identified using reduced velocity criterion [46], while in unsteady flow, there exist several methods [11]. The most popular coreline detection approach is via the Parallel Vector operator [28]. However, most

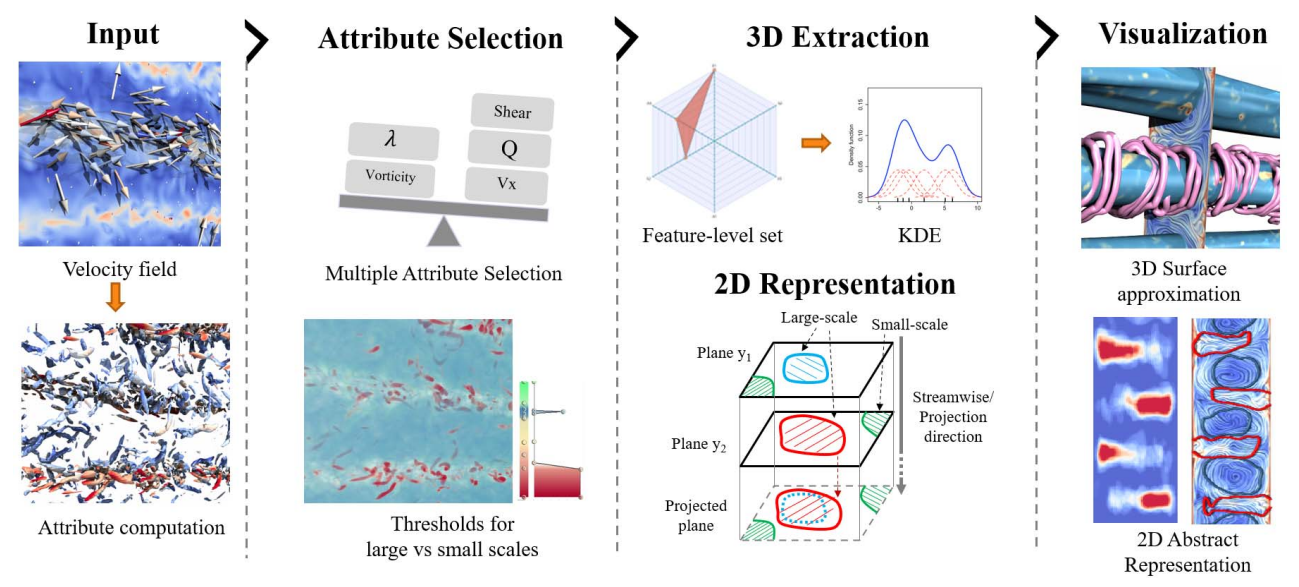


Fig. 4. The pipeline of our framework.

line-based methods are numerically unstable and easily result in fragmented corelines, which may be challenging to clean up. Geometric methods construct the skeleton of vortex tube. For 2D flows, Sadarjoen et al. [32,33] presented two geometric approaches based on the shape of streamlines. Their curvature center method computes the density of curvature centers for a given set of streamlines. Their second method uses winding angle of streamlines to identify regions of swirling flow. Streamlines having winding angles larger than a threshold are considered part of vortices. Again, selecting proper threshold is challenging. Objective methods aim to identify the optimal reference frame so that small-scale vortices can be revealed [11]. **Integration**based measures such as particle density estimation [48] and analyzing of Jacobian [46] were proposed to address the possible missing vortices with the above local method. Finally, there is a need to detect vortex **boundary** to measure the size of a vortex [11]. Haller et al. [12] proposed elliptic Lagrangian coherent structure (LCS), which preserves arc length and area in incompressible 2D flows and considered the outermost elliptic LCS, of a family of nested elliptic LCSs, as the boundary of a coherent vortex.

2.3 Multi-scale Processing of Flow Data

Given the increasing complexity of flow data and the multi-scale nature of the turbulence flow, multi-scale processing is required to delineate physical events arising across different scales. There are two types of multi-scale processing of flow data. The first group of methods construct the topological hierarchy of the velocity (or vector) fields. Both bottom-up and top-down strategies have been introduced. The bottomup strategy is usually realized as some simplification process, that gradually merges (or cancels) pairs of topological features, including fixed points [5, 6, 37, 38, 41, 43, 44, 47, 49] and periodic orbits [3], based on certain proximity (e.g., Euclidean or flow distance) between features. In contrast, the top-down approaches usually start with a coarse structure and gradually refine (or split) it. The top-down strategies are only seen in techniques based on Morse decomposition [2, 4, 40], where the structure with different fineness can be obtained with different particle advection times (i.e., a multi-valued flow map). Nonetheless, for turbulent flows, topology based approach may generate too many detailed structures that complicate the interpretation of the flow behavior.

Different from the above topology-based multi-scale processing, the non-topology-based methods define the scales in frequency space. Mundane methods of filtering out scales for coherent structure extraction, such as Fourier transforms [1, 10, 22] have been applied successfully. They have seen wide applications in homogeneous isotropic turbulence, and provided glimpses on how the real-world turbulent cascade oper-

ates. However, they are inherently non-local and are in practice limited to periodic and homogeneously discretized domains. Wavelet methods [7–9, 23] were developed to overcome the limitations of Fourier transforms, but have not seen widespread adoption in fluid mechanics. This is because for turbulence analysis, the wavelets considered rapidly become complicated and problem-specific instead of universal [34].

As the goal for the visualization of Taylor-Couette flows is to effectively separate the large-scale structures from the small-scale ones to facilitate its analysis, we adopt a feature level-set based strategy coupled with a density estimation, which is detailed next.

3 OUR METHOD

Overview. As stated earlier, our goal is to separate large-scale vortex structure from the small-scale ones and provide an intuitive and interactive visual representation so that fluid mechanics experts can quickly evaluate their hypotheses.

To achieve this goal, we propose a pipeline as illustrated in Figure 4. We first derive multiple attributes from the input velocity field. By analyzing the characteristics of the attributes in each cylinder rotation ratio and with knowledge from the expert, we select attributes and their corresponding value ranges that can partially indicate the existence and location of large- and small- scale structures (Section 3.1). To extract and visualize the structures in 3D, we adapt the recently introduced feature level-set [16] to compute a distance field to combine the selected attributes and their corresponding value ranges to better locate and separate large- and small- scale structures (Section 3.2). To achieve a smooth representation of the shape of the large- or smallscale structures, we further apply a kernel density estimation on the regions extracted from the obtained distance field (Section 3.3), from which a surface that approximates the geometric configuration of the large- or small- scale structure is extracted for visualization. Attribute information can be visualized on the extracted surface to provide additional information of the structure. To provide a summary view of the TCF in 2D, we project the areas in the individual 2D cross sections (parallel to the WS plane) with the attribute values falling within the respective selected value ranges onto the first cross section. This process is illustrated in Figure 4 under 2D Representation. This aggregated information is color coded on top of the LIC texture of the 2D flow in the first cross section. An example of this summary 2D visualization is shown in Figure 8 (e) and (f).

3.1 Attribute Selection

Physical attributes for the region-based vortex extraction. Given a steady vector field \mathbf{v} , its spatial gradient $\nabla_{\mathbf{x}}\mathbf{v}$ is referred to as its

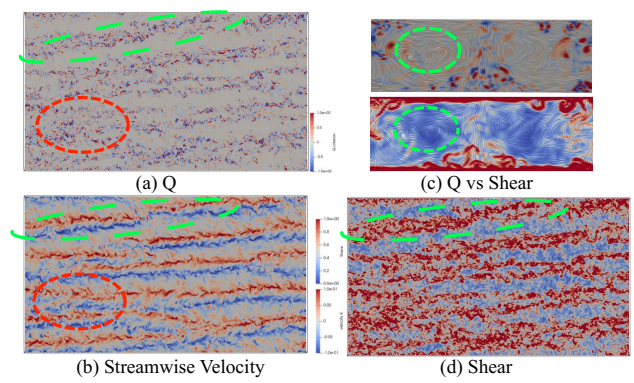


Fig. 5. Visualization of (a) O, (b) Streamwise velocity, (d) Shear in 2D cuts along the wall-normal direction, and (c) in the streamwise direction with $R_{\omega} = 0.05$. Q is noisier than the streamwise velocity and *Shear* in the wallnormal and streamwise directions and not able to separate structures with different scales here. By combining the streamwise velocity and Shear, we can better capture the prominent structures in both wall-normal and streamwise direction.

Jacobian, denoted by **J**. **J** can be decomposed as $\mathbf{J} = \mathbf{S} + \mathbf{R}$, where $\mathbf{S} =$ $\frac{1}{2}[\mathbf{J} + (\mathbf{J})^{\top}]$ and $\mathbf{R} = \frac{1}{2}[\mathbf{J} - (\mathbf{J})^{\top}]$ are the symmetric and anti-symmetric components of **J**, respectively. In addition to the velocity magnitude and the individual (u, v, and w) components of the velocity field, a number of flow attributes related to coherent structures, especially vortices, can be derived from \mathbf{v} , \mathbf{J} , \mathbf{S} and \mathbf{R} [29], such as:

• vorticity magnitude, $||\nabla \times \mathbf{v}||$.

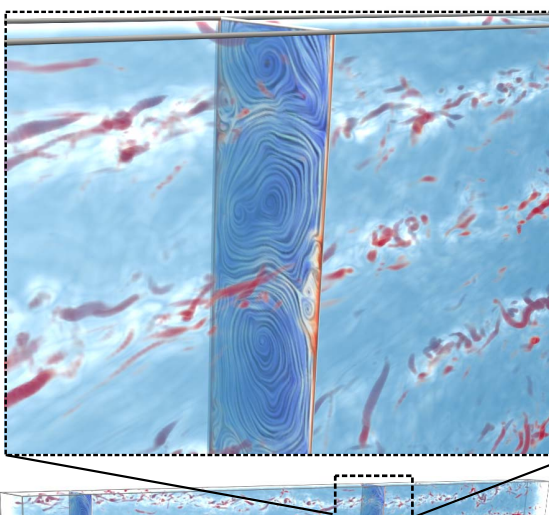
- λ_2 , computed as the second largest eigenvalue of the tensor S^2 + \mathbf{R}^{2} [17].
- $Q = \frac{1}{2}(\|\mathbf{R}\|^2 \|\mathbf{S}\|^2).$
- local shear rate, defined as the Frobenius norm of S.

These scalar attributes can help to identify regions of vortical behavior. For example, if the Euclidean norm of the vorticity tensor R is greater than the magnitude of strain rate tensor S, then the region contains a vortex. This criterion is equivalent with the condition Q > 0. The main drawback of the region-based methods is that the local attributes with a single threshold value tend to focus on smallscale features. Thus, the conventional thresholding approach is not sufficient for the extraction of large-scale structures. Nonetheless, for TCF, structures with different scales may be associated with certain value ranges of some attributes. By carefully selecting these ranges of certain attributes, small- and large-scale structures may be better separated for the subsequent processing.

In our pipeline, domain experts can select a single attribute, and then analyze it through statistical-based methods [18] or with the aid of volume rendering to obtain the desired value ranges which potentially reveal the location and shape of the coherent structures. As illustrated in Figure 2, small vortices can be extracted with Q > 2 for the simulation setting $R_{\omega} = 0.1$. In contrast, the large-scale structures can be observed via the volume rendering of Q with values $\in [0,0.1]$ (Figure 6). Interestingly, for TCF, we found a correlation between the rotation ratio R_{ω} and the value range of Q. In particular, we can use a value range of $[0,R_{\omega}]$ for Q to roughly reveal the large-scale structure. This observation is also confirmed previously [39].

In addition to the value selection for a single attribute, the experts can also select multiple attributes to better extract large-scale structures. The motivation for combining different attributes comes from the issue of using a single attribute like Q, which may only perform well in the TCF with a high cylinder rotation ratio R_{ω} . With lower rotation ratio, Q produces noisy data, making the extraction more difficult. As illustrated in Figure 5, Q is noisier than the streamwise velocity and *Shear* in the wall-normal and streamwise direction for $R_{\omega} = 0.05$. Either the streamwise velocity or Shear along is NOT sufficient in both directions; but by combining the features revealed by both the streamwise velocity and Shear, we can fully capture the prominent structures in the 3D configuration (Figure 11).

Even though we can see the assembling of the structures in the volume rendering after selecting the proper value ranges of certain



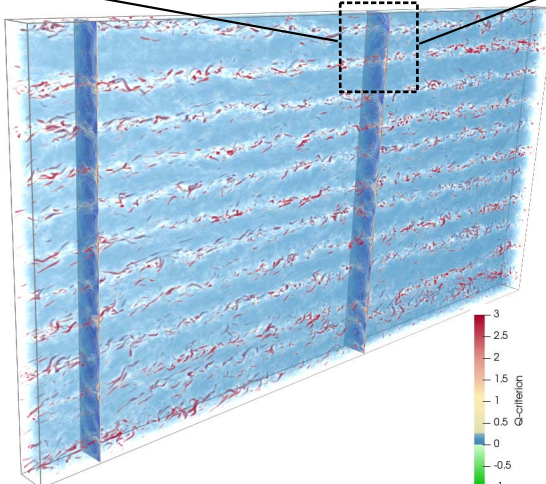


Fig. 6. Volume rendering of *Q*-criterion corresponding to the large-scale structures (blue with $Q \in [0,0.1]$) and small-scale structures (red with Q > 2), respectively.

attributes, as illustrated in Figure 6, effectively isolating and extracting them is not trivial. Next, we will describe how we address this challenge with the help of feature level-set extraction.

3.2 Feature Level-Set Extension

To extract 3D coherent structures, we adapt the feature level-set method to combine the characteristics of the selected attributes. Feature levelset is the generalization of the concept of level-set (i.e., iso-surface) from uni-variate to multi-variate data. It is superior to the method proposed by Schneider et al. [35] in which the authors try to find features in the spatial overlap of iso-surfaces extracted from two attributes. That method does not work if there is no intersection between the iso-surfaces. Feature level-set does not suffer from the issue. In the original version, feature level-set only works with a single (threshold) value for each attribute. We modify the distance metric so it can work with values within a range. Assume that we have N attributes $\mathscr{A} = \{a_1, a_2, \cdots, a_N\}$ for each point **p** in the spatial domain. We denote $\{\{v_{i,1}, v_{i,2}\} \mid v_{i,1} \leq v_{i,2}, i \in [1,N]\}$ as the selected value ranges for either small-scale or large-scale features for these attributes. The scalar distance or level to each point p is defined as follows:

$$d_{\mathbf{p}} = \begin{cases} 0, & \text{if } \exists i, a_i \in \left[v_{i,1}, v_{i,2}\right] \\ \min_{i \in \left[1,N\right]} \min \left\{ \left\|a_i - v_{i,1}\right\|, \left\|a_i - v_{i,2}\right\| \right\}, & \text{otherwise.} \end{cases}$$

Given the attribute thresholds for small- or large- scale features, the feature level-set outputs a distance field in which the regions with smaller distance value belong to the small- or large- scale structures. To increase the smoothness of the distance function, we attempted to replace the Frobenius norm with the sigmoid function. However, the result did not improve significantly. Frobenius norm is ultimately selected because of its high accuracy and low computational complexity. It is important to note that we normalize the attribute values before computing the distance field. Thus, all attributes are in the same range, making the distance comparison feasible.

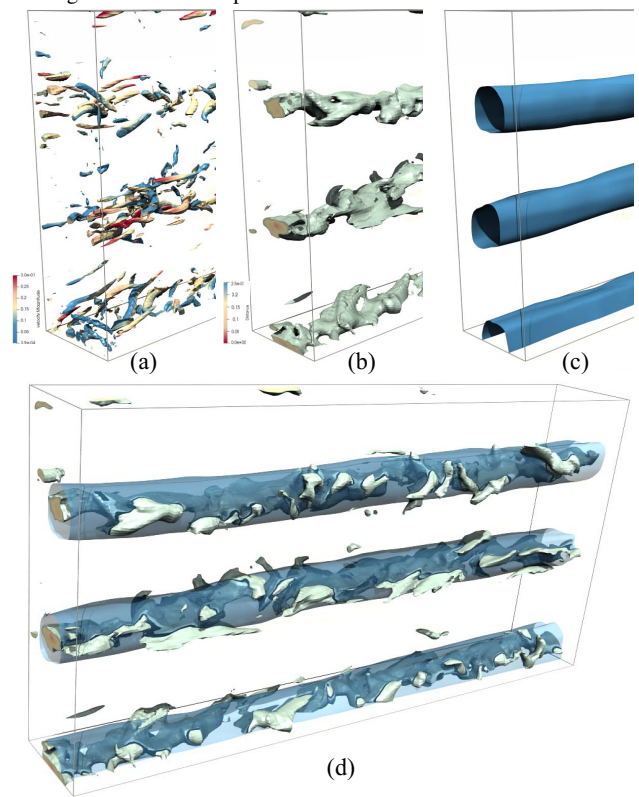


Fig. 7. Motivation for the kernel density estimation. (a) Original isosurfaces using Q-criterion lead to visual clutter. (b) The extracted isosurfaces from the distance field computed with the feature level-set. (c) Iso-surfaces extracted from the density field provide cleaner visualization. $\sigma=0.56,\ h=0.6,\ m=8.$ (d) The combined visualization of (b) and (c).

3.3 Kernel Density Estimation

Once we compute the distance field, the straightforward method to extract the surface representation for coherent structures is to apply iso-surfacing with a small distance threshold. In practice, however, the distance field is not always smooth as shown in Figure 7(b), leading to the disconnected and noisy iso-surfaces. To overcome this, we propose to group the (likely disconnected) regions that correspond to the large- (or small-) scale structures based on their spatial proximity, then provide the abstract visualization for each structure. To characterize their spatial distribution, we apply the kernel density estimation (KDE) to map the distance values into a density field in which higher density values correspond to the area containing more structures with similar scale. KDE was first proposed by [27], and it is a well-established method to achieve a non-parametric estimation for spatial density. We approximate the density function using a Gaussian kernel density estimate similar to [25] in a cube-like neighborhood area P centered at x with size $n = m^3$:

$$f(x) = \frac{1}{n(h\sqrt{2}\pi)^d} \sum_{i=1}^n exp(-\frac{||x-p_i||^2}{2h^2}) \times w$$
 (2)

with $||x-p_i||^2$ being the Euclidean distance between grid points, h being the bandwidth of KDE, d being the dimension of the grid. We utilize the Silverman method [36] to compute the optimal bandwidth which gives us $h = 1.06\sigma N^{-\frac{1}{5}}$ with σ the standard deviation and N

the number of grid points. Note that we assume the true distribution of the data is Gaussian. Compared to the conventional KDE, we add a weighing term, w, which sets the density values to zero for the grid points not enclosed by a large- (or small-) scale structure. A point belongs to a coherent structure if the distance value is zero. Thus, the value of the weight term w is equal to 1 if the distance value is zero, otherwise w = 0. We do not set w to the actual values of distance values because the purpose of KDE in this step is to reveal how dense the small distance values are in a certain neighborhood area. Based on the computed density field, iso-surfaces are extracted to provide a visual representation of large- (or small-) scale structure groups. As can be seen in Figure 7, we can derive three main groups for a sub-volume of the flow, which are represented by three large iso-surfaces (blue) in (c) from eighty nine small regions in (a). The density iso-surfaces provide a cleaner visualization.

3.4 Generate Composite Visualization

Selecting the threshold for KDE iso-surface is a trial and error process. Based on our experiments, however, we observe that setting the threshold to half of the density value range can produce a reasonable result. If the density value at a grid point is greater than the half of the value range, it means that the majority of its neighbors belong to the desired coherent structures. Half of the density value range is set by default for all of our results. The color of KDE iso-surfaces is mapped to one of the selected physical attributes in the feature level-set extraction step. A smooth color surface indicates a better physical alignment of the obtained surfaces.

Streamlines can be used to depict the flow motion, and verify the correctness of the extracted coherent structures as they should wrap around the structures in the simulation with high R_{ω} values. To generate a small set of such streamlines, we use a straight seeding rake that is close and parallel to the surface of the large (or small) scale structures. Some sample streamlines are shown in Figure 8(b)(d) and Figure 11. Combined with the extracted boundary surfaces, they provide a more informative visualization.

As we described in Section 2.1, the TC simulation is carried out in Cartesian coordinates where the cylindrical streamwise coordinate is unwrapped onto a straight line. To provide a more intuitive visualization, we wrap back the streamwise dimension from the straight to the cylindrical setting. Coordinate transformation is a widely solved math problem. Assume R_1 is the radius of the inner cylinder. We denote NX as the number of points in the streamwise direction, s_x , s_y , s_z are the spacings between two neighboring points along the streamwise, wall-normal, and spanwise directions, respectively. For each grid point (i,j,k) in the regular grid in the Cartesian space, we can derive the corresponding point (x,y,z) in the cylindrical coordinate as follows:

$$\begin{cases} x = r\cos(j*2\pi/NX) \\ y = r\sin(j*2\pi/NX) \\ z = ks_z \end{cases}$$
 (3)

where $r = R_1 + i * s_y$. R_1 is a user-specified value and can be obtained from the simulation spatial information. In our results, $R_1 = 4$.

4 RESULTS

We have applied our analysis and visualization framework to Taylor-Couette flows simulated with three different cylinder rotation ratios, $R_\Omega=0.1,0.05,0$ (Section 2.1), respectively. The velocity fields of these three simulations are stored in the VTK binary format with the size of 12GB each. In this section, we first demonstrate how the proposed framework can produce a first effective 3D visualization of TCF to depict the 3D behaviors of TCF. We then discuss how our 3D visualization helps domain experts analyze the 3D behaviors of TCFs with low cylinder rotation ratios (i.e., R=0.05 and R=0) that was not possible with the traditional 2D visualizations. We compare our method with the most widely used approach in multi-scale structure extraction – the convolution kernel filter, and point out a potential combination of the convolution kernel filter with the proposed method. Last but not least, we report the performance of our implementation.

TCF with $R_{\Omega} = 0.1$ **.** Figure 8 provides the visualization of the TCF with R = 0.1. It is known by the expert that the large-scale Taylor rolls

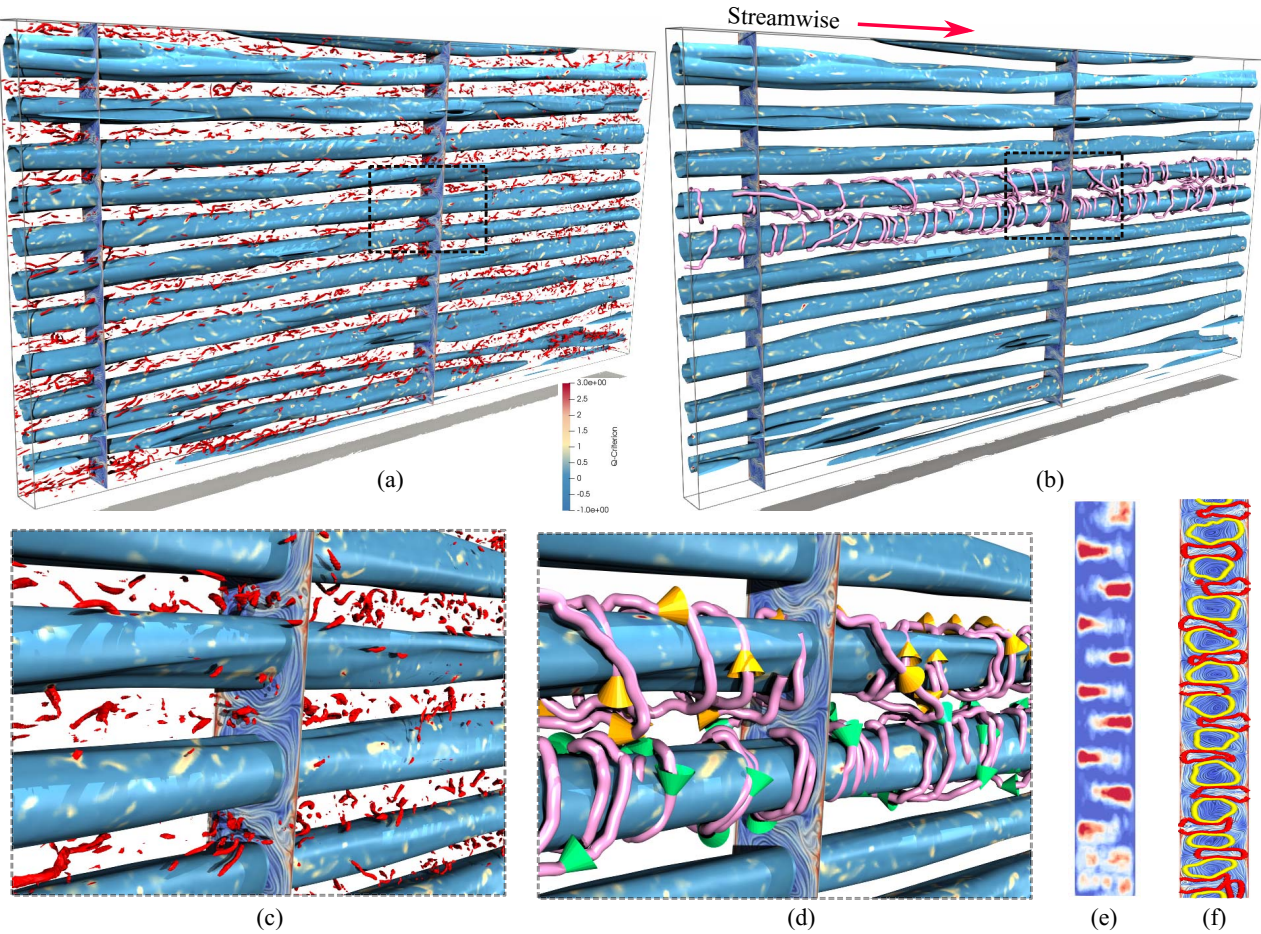


Fig. 8. Visualization of the large-scale structures for TCF with R=0.1. (a) shows the combined view of the small-scale vortices extracted with the threshold Q>2 (red) and the large-scale structures (blue) using the proposed method. (b) visualizes the large-scale structures that are alike Taylor rolls with streamlines swirling around them. The surface color is mapped to Q. The red arrow indicates the streamwise direction. (c)(d) provide the close-up views of (a) and (b), respectively. (e) A 2D abstract representation focuses on the high concentration of small-scale structures (red). (f) shows a **WS** plane with the LIC texture and the corresponding boundaries of the small- (red) and large- (yellow) scale structures.

are fully formed in this simulation. These large-scale Taylor rolls can be depicted by their corresponding Taylor vortices with opposite rotation in the 2D cross section. Figure 8(a) shows the combined visualization of the extracted small-scale vortices (the red iso-surfaces) and large-scale structures (the blue tubes). The closeup view is presented in Figure 8(c). From this overview visualization, the expert can easily see the configuration of the small- and large-scale structures that form interleaving spatial layout along spanwise direction. This is verified by the conventional 2D visualization (e.g., the LIC texture shown in Figure 8(f)). The feature level-set is computed by using the two attributes Q and the velocity magnitude in which $Q \in [0,0.1]$, and the velocity magnitude $\in [0.05,0.1]$.

Another prominent characteristic revealed in this visualization is that the large-scale structures (blue surfaces) are mostly following the streamwise direction (i.e., their orientation is aligned with the horizontal boundary). The red arrow indicates the streamwise direction in Figure 8(b). This characteristic is known as the *streamwise invariant* property of Taylor rolls, which means that the behavior of the flow on a cross section perpendicular to the streamwise direction is almost identical and independent of the location of the cross sectional cut along the streamwise direction. This is the reason why domain experts often use 2D visualization to study TCF with large cylinder rotation ratio. Nonetheless, 2D visualization emphasizes the large Taylor roll vortices as they are visually dominant in the LIC texture and may not capture the small-scale vortices that do not intersect with the 2D cross section.

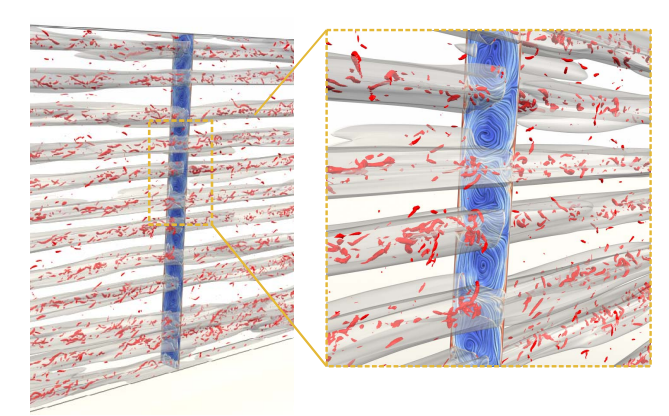
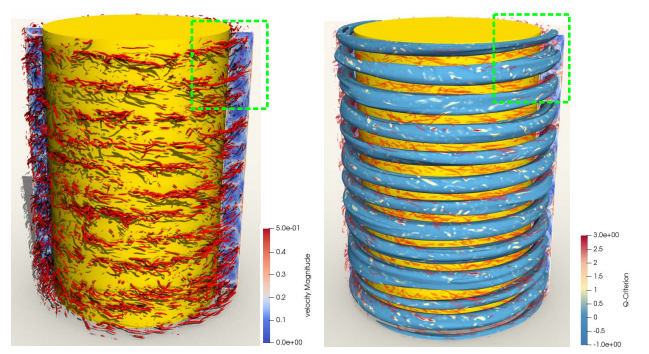
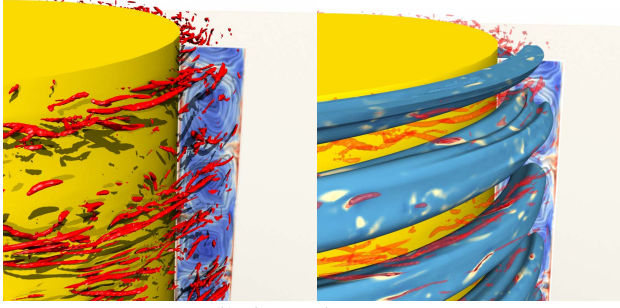


Fig. 9. Visualization of the regions (enclosed by transparent surfaces) with small-scale structures not belonging to the Taylor rolls for $R_{\omega}=0.1$.

To verify that the large-scale features extracted with our approach approximate the Taylor rolls in the TCF, we compute a number of streamlines along these features (Figure 8(b)). We see that these streamlines are swirling around the respective surfaces, indicating the rotation motion of the flow. The rotation bundles formed by these streamlines mostly match the geometry of the extracted surfaces. Figure



(a) Structures in the Cylindrical View



(b) Close-up view

Fig. 10. (a) Visualization of the small-scale (left) and large-scale (right) features in TCF with $\it R=0.1$ in the cylindrical coordinate reveals the well-known Taylor roll structure. (b) provides the close-up view for the small- (left) and large-scale (right) structures, respectively.

8(d) provides a closeup look. In addition to streamlines, we also color the extracted surfaces using the Q attribute measured on them. Our assumption is that if the color is close to constant on the surface, the surface is aligned well with the corresponding attribute. As can be seen in the provided visualization, most parts of the surfaces have similar colors except for a few spots, indicating a good alignment with the Q attribute. In summary, our visualization demonstrates that the extracted surfaces do approximate the Taylor rolls.

When compared to the 3D visualization using simple thresholding shown in Figure 2, our visualization provides a much cleaner separation of the regions dominated by the small-scale and large-scale features, respectively. It also enables the depiction of the large-scale flow motion, which is not easy to capture with the local physical attributes (i.e., vorticity, Q, and/or λ_2). This is because this large-scale motion corresponds to low values of those physical attributes. Our method can successfully identify them.

Figure 8(e) shows a density field which is computed based on the projection of small-scale structures onto a 2D cross section of the streamwise axis (i.e., parallel to the WS plane). N_x cross sections uniformly distributed in the streamwise direction are used ($N_x = 512$ in our experiments). The places with high concentration of the density field (i.e., corresponding to regions where more small-scale features reside) coincide with the places with high velocity magnitude (f). Note that this density field visualization indicates that the majority of the small-scale structures stays close to the boundary and form a clear periodic spatial distribution layout, indicating the formation of the Taylor rolls/vortices. Such a summary view is not easily obtained with the conventional approach.

With the separation of the regions with small-scale and large-scale structures, the expert can now study their different behavior separately. While Figure 8(b) focuses on large-scale structures, Figure 9 reveals the detailed behavior of the small-scale structures. The red iso-surfaces represent the small vortices extracted by using the threshold Q>2. The gap between the 3D transparent surfaces that enclose all small vortices are the places where 3D Taylor rolls reside.

To enable an intuitive understanding of TCF in the real-world setting (Figure 1), we transform the extracted features with our method to a

cylindrical coordinate system. Figure 10 provides such a visualization. Specifically, Figure 10 (a) provides the entire flow in the cylindrical view for both small-scale (left) and large-scale (right) features. Figure 10 (b) provides a close-up view.

TCF with $R_{\Omega} = 0.05$. Next, we apply our framework to a TCF with $R_{\Omega} = 0.05$ (i.e., half of the rotation ratio used to generate the above TCF). This TCF is less ordered than the one seen above with $R_{\Omega}=0.1$. As shown in Figure 5 (a), Q attribute is not sufficient in capturing the large-scale structures in this case. By examining other attributes, we found that both local shear rate and the streamwise velocity can reveal a cleaner configuration of the large-scale structure (Figure 5 (b)(d)). Therefore, we use these two attributes in the feature level-set computation. The value ranges for these two attributes are [0.05, 0.2]for the streamwise velocity and [0.8, 2] for shear, respectively. Figure 11 (b) shows the overview of the flow with the red small vortices identified with Q = 2. Compared to the TCF with $R_Q = 0.1$ (Figure 2), these small-scale vortices are less structured (in other words, more chaotic). Figure 11 (a)(c) show the visualization of this TCF using our framework. As can be seen, the identified approximate boundary surfaces of the large structures (curious blue) are not fully connected. This indicates the insufficient separation of the large-scale structures from the small-scale vortices, suggesting that the Taylor roll is not fully formed. This is better conveyed in the projected density field of the small-scale features shown in Figure 11 (g)(h), in which the high concentration of small-scale features (in red) are less structured and rather noisy. Nonetheless, these large structures still resemble Taylor rolls seen in the TCF with $R_{\Omega} = 0.1$. This is indicated by the seeded streamlines (Figure 11(c)). These streamlines still warp around the extracted surfaces, though not well-organized. Figure 11(f) offers a closeup look at these streamlines. Again, we color the extracted surface using one of the selected attributes (shear in this case). Based on the color distribution shown on the surface, we can see that the geometry of the surfaces aligns well with the local shear rate of the flow.

TCF with $R_{\Omega}=0.0$. Finally, we apply our method to the TCF simulated with $R_{\Omega}=0.0$. This is the most chaotic scenario in which the rotation is minimum. As shown in Figure 12(a), the small-scale vortices extracted using Q criterion cover almost the entire domain, making the separation of the large- and small- scale structures using attribute Q impossible. It is also known to the experts that there are no Taylor rolls in this TCF. Nonetheless, there may still exist other large-scale coherent structures. To reveal them, we again employ local shear rate and the streamwise velocity to compute the feature level-set for the extraction of the large-scale structure. The value ranges for these two attributes used here are [0.075, 0.15] for the streamwise velocity and [2.0, 5.0] for shearing, respectively.

Figure 12(b) visualizes the extracted surfaces approximating the large-scale structures. The streamline seeded at one of the surfaces corresponding to the large-scale structure has nearly flat geometry (i.e., not circulating around the corresponding surface as seen in the previous TCF results). This indicates that the flow motion at or near these large-scale structures is not rotational, which in turn shows that these structures are NOT Taylor rolls.

Expert evaluation. We have shown our results to an expert from the fluid mechanics community. In his impression, the visualization for the TCF with $R_\Omega=0.1$ adequately captures the regions of vortex generation, and the "quiet" regions. Furthermore, the method is able to summarize the regions where vortices are formed from small-scale data, and this shows promise for application in a wide variety of problems like thermal convection, shear flows and wall turbulence. More impressively, the method is also able to extract the coarse-grain regions where the large-scale rolls are not streamwise invariant, but show a more complicated geometry (e.g., for the TCF with $R_\Omega=0.05$), providing a rapid intuition of where transport barriers can arise.

In addition, the expert pointed out that our 3D visualization enables a more thorough inspection of the 3D behaviors of TCFs that were not possible with his existing 2D visualizations. Specifically, when $R_{\Omega} = 0.1$, each Taylor roll rotates in the opposite direction to its neighboring rolls, as observed in the respective 2D cross sections (Figure1(a)). The circulating motion of the flow is nicely depicted by the sampled streamlines that wrap around the extracted tubular struc-

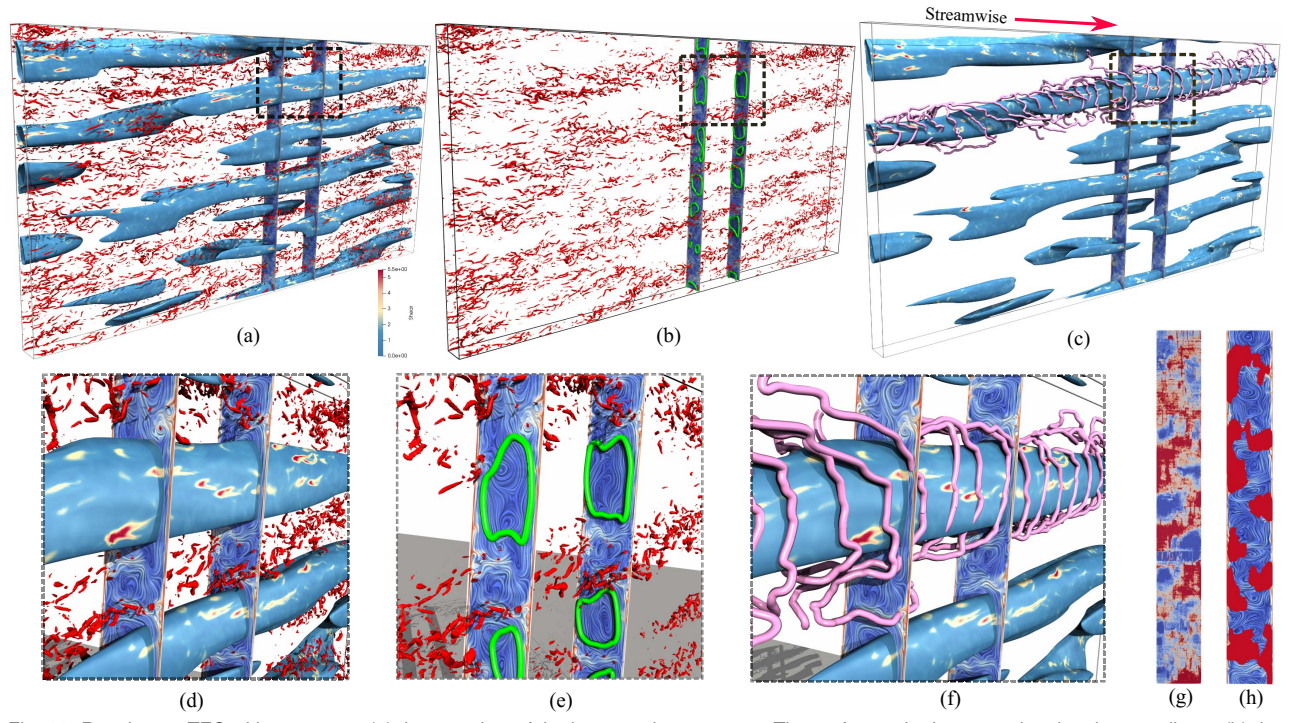


Fig. 11. Result on a TFC with $R_{\Omega}=0.05$. (a) the overview of the large-scale structures. The surface color is mapped to the shear attribute. (b) the small-scale vortices (in red) extracted with Q=2, and slice cuts show the intersection of large structures and the WS planes. (c) streamlines wrap around a large structure. (d)(e)(f) provide the closeup views at the corresponding black rectangles in (a)(b)(c). (g) 2D abstraction representation indicates the regions with high concentration of the small structures, and (h) the projection of the small structures (red) on a LIC texture.

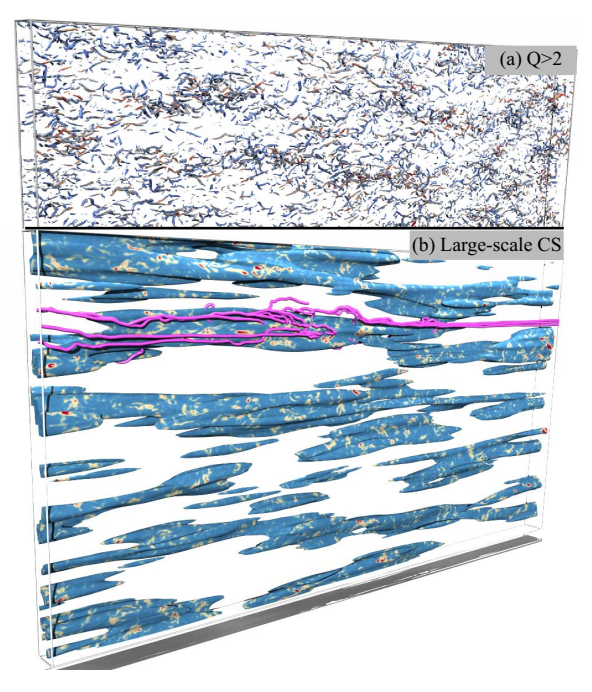


Fig. 12. Visualization of (a) the vortices extracted by using the threshold Q>2 for a TCF simulation with $R_\omega=0$. It is impossible to visually distinguish the difference between the large- and small- scale structures as the vortices are distributed everywhere in the spatial domain, and the Taylor rolls are not clearly formed. (b) The large-scale structures are extracted using local shear rate and the streamwise velocity. The seeded streamlines (magenta) in the bottom have an overall flat configuration, indicating the absence of Taylor rolls.

ture, which give an idea of how many wraparounds happen as the fluid particles transverse the flow. This large-scale configuration is relatively streamwise invariant (i.e., they are not shifting up and down) and remain stable in streamwise direction. In contrast, when $R_\Omega=0.05$, the large-scale structure extracted is not streamwise invariant (moving up and/or down). In addition, this structure is not always connected along streamwise direction. This indicates the well-shaped Taylor rolls as seen in the $R_\Omega=0.1$ simulation are not formed. In this case, inspecting only 2D cross sections of the flow is not sufficient, as some cross sections may have well-shaped vortices while the others do not.

For TCF with $R_{\Omega}=0$, there is no existing method that can effectively isolate the large-scale structures from the small ones. Although the proposed method does not completely overcome this challenge, the extracted surfaces partially reveal the shapes and positions of the structures that the expert hypothesizes. This suggests that the proposed framework can be applied to a more systematic study on how R_{Ω} impacts the configuration of Taylor rolls and to identify the threshold value of R_{Ω} that leads to the fully developed Taylor rolls.

Although the presented method is able to isolate the Taylor roll successfully, the robustness of the isolation of the vortex remains to be properly assessed, and in the expert's opinion we have to go beyond visualization to quantify several aspects of the roll dynamics, such as its energy and position through time. The current approach cannot accurately capture the Taylor rolls for their quantitative analysis. Nonetheless, the expert believes that the method developed here could be used as springboard for low-order modelling of these structures, a very relevant research aim of the turbulence community in the present.

Comparison with the convolution kernel approach. To demonstrate the advantage of our framework over the traditional methods that usually perform smoothing to remove small-scale features, we compare our result with the most commonly used convolution kernel approach [42]. Figure 13 (b) shows the results using a convolution kernel - usually an averaging box filter with a kernel size of $12 \times 12 \times 12$ to the velocity field. Although the convolution kernel can generate a smoother result and better-connected surfaces, our approach aligns better with physics.

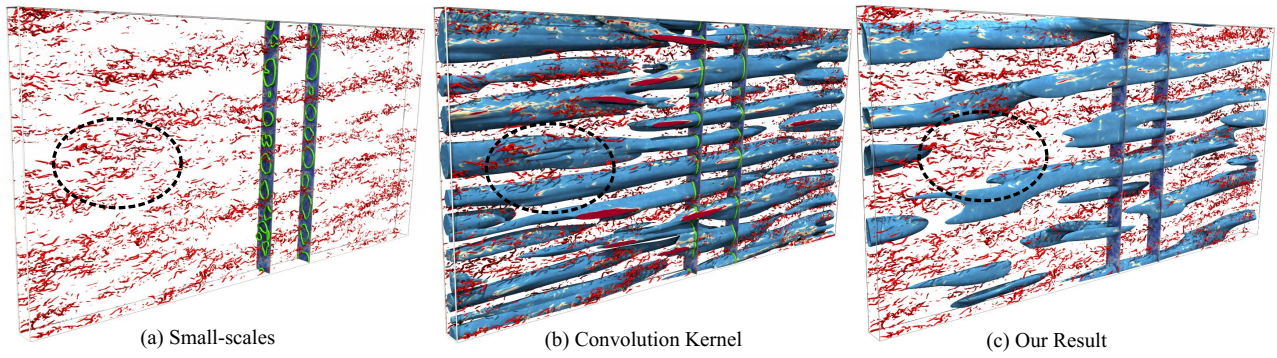


Fig. 13. Comparison with the convolution kernel on a TFC with $R_{\Omega} = 0.05$. The large-scale structures extracted with the convolution kernel falsely includes an area occupied by small-scale features. In contrast, our method correctly excludes this region from the extracted large-scale structure.

This is because the convolution kernel may falsely enclose areas that are occupied by small-scale features. As highlighted by a black dashed circle in Figure 13, a region that is dominated by the small-scale vortices becomes part of the large-scale structure after applying convolution kernel (Figure 13 (b)). In contrast, our method correctly detects this area and excludes it from the construction of the large-scale structure. In addition, we can see that the attribute values on the surfaces extracted using the convolution kernel have large variations (e.g., a few large areas colored in red on the those surfaces, indicating that the geometry there does not align well with the physical attribute (i.e., those parts should not belong to the extracted structure).

Performance. All numerical experiments reported are carried out on a PC with an Intel Core i7-9750H CPU, 128GB DDR3 RAM and a NVIDIA GeForce GTX1660Ti 6G graphic card. The framework is implemented with C++, and we use CUDA to parallelize the attribute, feature level-set and KDE computations. Note that the computation at each grid point is independent from the other points; hence, the computational complexity is reduced from N^3 for the sequential implementation (N is the spatial resolution in each dimension) to nearly a constant for our parallelized version.

Parameter discussion. Our approach depends on two types of parameters, i.e., the value ranges of the selected attributes, the neighborhood size m for the KDE computation and the iso-value for surface extraction. The discussion on how to properly select value ranges for the feature level-set computation is provided in Section 3.1. For the KDE computation, the larger m is, the smoother the obtained surfaces will be. However, if m is too large, the density field can be overly smoothed, resulting in connected large-scale features (an example is provided in the supplemental document). Based on our experiments, m = 10usually yields the best results. To extract the iso-surfaces with an ideal covering percentage of coherent structures, the iso-value is set to half of the density value range. An example showing surfaces extracted using different iso-values is provided in the supplemental document. Table 1 reports the optimal KDE parameter values and the optimal covering percentages (explained next) of large-scale structures for the three TCFs described above.

Accuracy measurement. To measure the accuracy of our results, we compute two covering percentages: (1) the percentage of the large-scale structures enclosed by the obtained surfaces and (2) the percentage of the small-scale structures enclosed by the surfaces. The former is computed as the ratio between the number of voxels enclosed by the surfaces that intersect with the large-scale structures (determined by the value ranges of the selected attributes) and the number of voxels in the entire domain that intersect with large-scale structures. This essentially estimates the true positive (TP). The latter is computed as the ratio between the number of voxels enclosed by the surfaces that intersect with the small-scale structures and the number of all voxels enclosed by the surfaces. This is measuring the false positive (FP). An ideal surface should have TP close to 100% and FP close to 0. Table 1 reports the accuracy measurement of our results. As a comparison, the TP and FP values for the convolutional kernel result shown in Figure 13 (b) are

92.32% and 18.4%, respectively. Although it achieves slightly better coverage of large-scale structures than our result (Figure 13 (c)), it covers significantly more small-scale structures than it should, which makes it less accurate than our result.

Table 1. Parameters used for all TCFs with m=10 and their accuracy mass unmost

measur	ement.

R_{Ω}	Bandwidth	Iso-values	Large-scale CS covering (TP)	Small-scale CS covering (FP)
0.1	0.72	0.061	94.4%	7.3%
0.05	0.60	0.050	89.8%	9.5%
0.0	0.42	0.043	85.7%	17.6%

5 CONCLUSION

In this paper, we present a framework for the visualization and analysis of Taylor-Couette flow (TCF), a well-known turbulence flow that is frequently studied in various situations. However, existing methods cannot effectively separate the large-scale structures (i.e., Taylor rolls/vortices) from the dense, space-filling small-scale structures for the study of transport barriers. To address this issue, we propose a novel visualization framework. First, we derive physical attributes, and find a combination among these attributes via the feature level-set technique to better capture the difference between the large- and small- scale features. Second, we extract the iso-surface from the kernel density estimation of the distance field obtained from the feature level-set computation. We also provide 2D abstract representation through the plane projection along the streamwise direction to highlight the concentrated positions of structures with different scales. Our method is simple yet effective, enabling the separation of the large-scale structures from the smaller ones. It leads to cleaner visualization of this turbulence flow, facilitating its analysis for the experts. We have applied our framework to three TCFs simulated with different parameters to assess its effectiveness. We show that our framework can be used to distinguish TFC with different configurations.

Though we successfully separate regions with small-scale features from those with large-scale ones for TCF, there are still a number of limitations that need to be addressed in the future. First, the quality of the extracted surface representation for large-scale structures still depends on the proper selection of the value ranges of certain relevant attributes. This is not trivial and the thresholds can be arbitrary, as criticized by the expert. Second, we do not really extract the large-scale structures precisely, instead, we only provide an approximation on the regions where they may reside. In the meantime, the expert wishes to see the more accurate transport barriers of this flow, i.e., the boundaries of Taylor rolls, to quantify their dynamics. Finally, we focus on one time step for each TCF despite TCFs are unsteady flows. Nonetheless, the efficient computation of our framework enables us to explore an in-situ visualization and analysis of TCFs during their simulations. We plan to address these limitations in the future work.

ACKNOWLEDGMENTS

We thank the anonymous reviewers for their valuable suggestions. This research was supported by NSF IIS 1553329.

REFERENCES

- G. K. Batchelor. The theory of homogeneous turbulence. Cambridge university press, 1953.
- [2] G. Chen, Q. Deng, A. Szymczak, R. S. Laramee, and E. Zhang. Morse set classification and hierarchical refinement using conley index. *IEEE Trans. Vis. Comput. Graph.*, 18(5):767–782, 2012.
- [3] G. Chen, K. Mischaikow, R. S. Laramee, P. Pilarczyk, and E. Zhang. Vector Field Editing and Periodic Orbit Extraction Using Morse Decomposition. *IEEE Transactions on Visualization and Computer Graphics*, 13(4):769–785, Jul./Aug. 2007.
- [4] G. Chen, K. Mischaikow, R. S. Laramee, and E. Zhang. Efficient Morse Decompositions of Vector Fields. *IEEE Transactions on Visualization and Computer Graphics*, 14(4):848–862, Jul./Aug. 2008.
- [5] W. de Leeuw and R. van Liere. Visualization of Global Flow Structures Using Multiple Levels of Topology. In *Data Visualization '99 (VisSym '99)*, pp. 45–52. May 1999.
- [6] W. C. de Leeuw and R. van Liere. Collapsing flow topology using area metrics. In D. Ebert, M. Gross, and B. Hamann, eds., *IEEE Visualization* '99, pp. 349–354. San Francisco, 1999.
- [7] M. Farge. Wavelet transforms and their applications to turbulence. Annual review of fluid mechanics, 24(1):395–458, 1992.
- [8] M. Farge, N. Kevlahan, V. Perrier, and E. Goirand. Wavelets and turbulence. *Proceedings of the IEEE*, 84(4):639–669, 1996.
- [9] M. Farge, G. Pellegrino, and K. Schneider. Coherent vortex extraction in 3d turbulent flows using orthogonal wavelets. *Physical Review Letters*, 87(5):054501, 2001.
- [10] U. Frisch. Turbulence: the legacy of AN Kolmogorov. Cambridge university press, 1995.
- [11] T. Günther and H. Theisel. The state of the art in vortex extraction. Computer Graphics Forum, 37(6):149–173, 2018. doi: 10.1111/cgf.13319
- [12] G. Haller, A. Hadjighasem, M. Farazmand, and F. Huhn. Defining coherent vortices objectively from the vorticity. *Journal of Fluid Mechanics*, 795:136–173, 2016.
- [13] M. L. Hosain, R. Bel Fdhila, and K. Rönnberg. Taylor-Couette flow and transient heat transfer inside the annulus air-gap of rotating electrical machines. *Applied Energy*, 207(C):624–633, 2017.
- [14] S. G. Huisman, R. C. A. van der Veen, C. Sun, and D. Lohse. Multiple states in highly turbulent taylor-couette flow. *Nature Communications*, 5(1):3820, 2014. doi: 10.1038/ncomms4820
- [15] J. C. Hunt, A. Wray, and P. Moin. Eddies, streams, and convergence zones in turbulent flows. In *Studying Turbulence Using Numerical Simulation Databases*, 2, vol. 1, pp. 193–208, 1988.
- [16] J. Jankowai and I. Hotz. Feature level-sets: Generalizing iso-surfaces to multi-variate data. *IEEE Transactions on Visualization and Computer Graphics*, 26(2):1308–1319, 2020.
- [17] J. Jeong and F. Hussain. On the identification of a vortex. *Journal of fluid mechanics*, 285:69–94, 1995.
- [18] D. Krug, X. I. A. Yang, C. M. de Silva, R. Ostilla-Mónico, R. Verzicco, I. Marusic, and D. Lohse. Statistics of turbulence in the energy-containing range of taylor–couette compared to canonical wall-bounded flows. *Jour-nal of Fluid Mechanics*, 830:797–819, Oct 2017. doi: 10.1017/jfm.2017. 625
- [19] R. Laramee, H. Hauser, L. Zhao, and F. H. Post. Topology based flow visualization: the state of the art. In *Topology-Based Methods in Visualiza*tion (Proceedings of Topo-in-Vis 2005), Mathematics and Visualization, pp. 1–19. Springer, 2007.
- [20] R. S. Laramee, H. Hauser, H. Doleisch, F. H. Post, B. Vrolijk, and D. Weiskopf. The state of the art in flow visualization: dense and texturebased techniques. *Computer Graphics Forum*, 23(2):203–221, June 2004.
- [21] H. J. Lugt. The dilemma of defining a vortex. In Recent developments in theoretical and experimental fluid mechanics, pp. 309–321. Springer, 1979.
- [22] A. S. Monin and A. M. Yaglom. Statistical fluid mechanics, volume II: mechanics of turbulence, vol. 2. Courier Corporation, 2013.
- [23] J.-F. Muzy, E. Bacry, and A. Arneodo. Wavelets and multifractal formalism for singular signals: Application to turbulence data. *Physical review letters*, 67(25):3515, 1991.
- [24] M. Nemri, E. Climent, S. Charton, J.-Y. Lanoë, and D. Ode. Experimental and numerical investigation on mixing and axial dispersion in taylor–couette flow patterns. *Chemical Engineering Research and Design*, 91(12):2346 2354, 2013. doi: 10.1016/j.cherd.2012.11.010
- [25] P. Oesterling, C. Heine, H. Janicke, G. Scheuermann, and G. Heyer. Visual-

- ization of high-dimensional point clouds using their density distribution's topology. *IEEE Transactions on Visualization and Computer Graphics*, 17(11):1547–1559. Nov 2011. doi: 10.1109/TVCG.2011.27
- [26] R. Ostilla Monico. Highly turbulent Taylor-Couette flow: direct numerical simulations. PhD thesis, University of Twente, 2 2015. doi: 10.3990/1. 9789036537995
- [27] E. Parzen. On estimation of a probability density function and mode. Ann. Math. Statist., 33(3):1065–1076, 09 1962. doi: 10.1214/aoms/1177704472
- [28] R. Peikert and M. Roth. The "parallel vectors" operator-a vector field visualization primitive. In *Proceedings Visualization '99 (Cat. No.99CB37067)*, pp. 263–532, Oct 1999. doi: 10.1109/VISUAL.1999. 809896
- [29] A. Pobitzer, A. Lez, K. Matkovic, and H. Hauser. A statistics-based dimension reduction of the space of path line attributes for interactive visual flow analysis. In *PacificVis*, pp. 113–120, 2012.
- [30] S. K. Robinson. Coherent motions in the turbulent boundary layer. Annual Review of Fluid Mechanics, 23(1):601–639, 1991.
- [31] F. Sacco, R. Verzicco, and R. Ostilla-Mónico. Dynamics and evolution of turbulent taylor rolls. *Journal of Fluid Mechanics*, 870:970–987, May 2019. doi: 10.1017/jfm.2019.317
- [32] I. A. Sadarjoen and F. H. Post. Geometric methods for vortex extraction. In *Data Visualization* '99, pp. 53–62. Springer, 1999.
- [33] I. A. Sadarjoen and F. H. Post. Detection, quantification, and tracking of vortices using streamline geometry. *Computers & Graphics*, 24(3):333– 341, 2000.
- [34] T. Sakurai, K. Yoshimatsu, K. Schneider, M. Farge, K. Morishita, and T. Ishihara. Coherent structure extraction in turbulent channel flow using boundary adapted wavelets. *Journal of Turbulence*, 18(4):352–372, 2017.
- [35] D. Schneider, A. Wiebel, H. Carr, M. Hlawitschka, and G. Scheuermann. Interactive comparison of scalar fields based on largest contours with applications to flow visualization. *IEEE Transactions on Visualization and Computer Graphics*, 14(6):1475–1482, 2008.
- [36] B. Silverman. Density Estimation for Statistics and Data Analysis. Chapman & Hall/CRC Monographs on Statistics & Applied Probability. Taylor & Francis, 1986.
- [37] P. Skraba, P. Rosen, B. Wang, G. Chen, H. Bhatia, and V. Pascucci. Critical point cancellation in 3d vector fields: Robustness and discussion. *IEEE transactions on visualization and computer graphics*, 22(6):1683–1693, 2016.
- [38] P. Skraba, B. Wang, G. Chen, and P. Rosen. Robustness-based simplification of 2d steady and unsteady vector fields. *IEEE Transactions on Visualization and Computer Graphics*, 21(8):930–944, 2015.
- [39] V. Spandan, R. Ostilla-Monico, D. Lohse, and R. Verzicco. Identifying coherent structures and vortex clusters in taylor-couette turbulence. *Journal of Physics: Conference Series*, 708:012006, apr 2016. doi: 10. 1088/1742-6596/708/1/012006
- [40] A. Szymczak and E. Zhang. Robust morse decompositions of piecewise constant vector fields. *IEEE Transactions on Visualization and Computer Graphics*, 18(6):938–951, June 2012. doi: 10.1109/TVCG.2011.88
- [41] H. Theisel, C. Rössl, and H.-P. Seidel. Compression of 2D Vector Fields Under Guaranteed Topology Preservation. In *Eurographics (EG 03)*, vol. 22(3) of *Computer Graphics forum*, pp. 333–342, Sept. 1–6 2003.
- [42] M. Treib, K. Bürger, F. Reichl, C. Meneveau, A. Szalay, and R. Westermann. Turbulence visualization at the terascale on desktop pcs. *IEEE Transactions on Visualization and Computer Graphics*, 18(12):2169–2177, 2012.
- [43] X. Tricoche, G. Scheuermann, and H. Hagen. A topology simplification method for 2d vector fields. In *Proceedings of IEEE Visualization 2000*, pp. 359–366. IEEE Computer Society Press, Los Alamitos, CA, USA, 2000
- [44] X. Tricoche, G. Scheuermann, and H. Hagen. Continuous topology simplification of planar vector fields. In *Proceedings of IEEE Visualization* 2001, pp. 159–166, 2001.
- [45] E. P. van der Poel, R. O. Mónico, J. Donners, and R. Verzicco. A pencil distributed finite difference code for strongly turbulent wall-bounded flows, 2015.
- [46] T. Weinkauf and H. Theisel. Streak lines as tangent curves of a derived vector field. *IEEE Transactions on Visualization and Computer Graphics*, 16(6):1225–1234, 2010.
- [47] T. Weinkauf, H. Theisel, K. Shi, H.-C. Hege, and H.-P. Seidel. Extracting higher order critical points and topological simplification of 3d vector fields. In *IEEE Vis*, pp. 559–566, 2005.
- [48] A. Wiebel, R. Chan, C. Wolf, A. Robitzki, A. Stevens, and G. Scheuer-

- mann. Topological flow structures in a mathematical model for rotation-mediated cell aggregation. In *Topological Methods in Data Analysis and Visualization*, pp. 193–204. Springer, 2011.
 [49] E. Zhang, K. Mischaikow, and G. Turk. Vector field design on surfaces. *ACM Transactions on Graphics*, 25(4):1294–1326, 2006.